Theoretical and experimental investigation into an adjustable automotive damper

D J Purdy
Engineering Systems Department, Royal Military College of Science, Cranfield University, Shrivenham, Swindon SN6 8LA, UK

Abstract: A non-linear model of an adjustable automotive damper is developed, which includes the compressibility of the fluid, trapped gas and expansion of the cylinder. The parameters for the model are selected by fitting the model to experimentally obtained data from the damper. The model is shown to give an excellent representation of the damper under investigation. The performance of the damper model is examined as the parameters are varied, and the results are discussed.

Keywords: adjustable automotive damper, modelling, simulation, testing, parameter estimation

NOTATION

a	area (m^2)
c	linear damping coefficient (N s/m)
d	diameter (m)
f	force (N)
k	linear stiffness (N/m)
K_B, K_c, K_g	bulk modulus for fluid, cylinder and gas (N/m^2)
l	length (m)
m	mass (kg)
P	pressure (N/m^2)
q	flowrate (m^3/s)
R_m	valve mass flow restriction coefficient ($s\sqrt{N}/m\,kg$ or $N\,s/m^2\,kg$)
R_v	valve volume flow restriction coefficient ($N\,s/m^5$)
t	time (s)
V	volume (m^3)
x	displacement (m)
α	cubic expansion coefficient ($\mu m/m\,K$)
γ	adiabatic index
η	displacement of the gas piston (m)
ρ	density (kg/m^3)
ω	frequency (rad/s)

Superscripts

s	damper setting

Subscripts

0	initial conditions
1, 2, 3	relating to chambers or valves 1, 2 and 3 (see Figs 1 and 2)
c	cylinder
d	damper
f	friction
g	gas accumulator
p	damper piston
r	damper rod
v	vapour

The MS was received on 22 April 1999 and was accepted after revision for publication on 16 July 1999.

1 INTRODUCTION

A conventional suspension system for a wheeled vehicle consists of mechanical springs and dampers and has several functions to perform. Two of its main functions are to isolate the body from the terrain over which it is travelling and to keep the tyre in contact with the surface. The characteristics of these components are fundamental to the performance of the suspension system in achieving these objectives. In this paper the dynamics of an adjustable gas-pressurized damper are examined both experimentally and theoretically.

The objective of this research is to develop a parametric model of an adjustable damper that can be used to understand its dynamic characteristics and for vehicle simulation purposes. An understanding of its characteristics and how they are dependent on its design is important. This is because it can aid the designer in tuning damper performance for different vehicle applications. The adjustable damper chosen for this investigation has twenty discrete settings.

The most detailed study of an automotive damper in the literature was by Lang [**1**]. This was a very complex non-linear model of a non-adjustable unit, which had

over 80 parameters needing to be selected. It was simulated on an analog computer at a high stoking frequency and the results were compared with experimental data. There was a high degree of correlation between the model and the experimental data, though even on the analog computer the model showed signs of instability at times. The level of complexity and the necessity to determine large numbers of parameters experimentally make this model unsuitable as a design tool or for suspension investigations. The model by Lang [**1**] has been modified by Hall and Gill [**2**] for digital computer simulation. Simpler physical models of non-adjustable dampers have been proposed by Karadayi and Masada [**3**], Hagedorn and Wallaschek [**4**], Wallaschek [**5**] and Surace *et al.* [**6**].

A non-linear model of an automotive damper was proposed by Karadayi and Masada [**3**], using the describing function method. The final model produced consisted of a linear spring, linear damper and backlash in series. The backlash was used to represent the compressibility of the fluid. The results from this model showed good correlation with experimental results at low frequency (0.2 Hz).

A series of non-linear models was developed by Wallaschek [**5**] and similarly by Hagedorn and Wallaschek [**4**]. The final version of these models had nine adjustable parameters. These related to laminar flow, throttle losses, Coulomb friction and backlash for both bump and rebound. The backlash was again introduced to account for the compressibility of the fluid. The large number of parameters requiring selection and the modelling of compressibility by backlash make it difficult to use.

The compressibility of the fluid was introduced into a model by Surace *et al.* [**6**]. Although the geometry of the damper modelled was unconventional, it was used to highlight how the fluid compressibility and flow affected its performance. The results generated by simulation exhibited the general characteristics of a typical damper, but no experimental results for the damper were given.

This paper starts by describing the adjustable damper under investigation and developing a non-linear model with five tuneable parameters. The response of the model is examined for one of the settings and then the parameters for the damper are estimated for the 20 settings. Finally, the results are discussed and conclusions are drawn.

2 DESCRIPTION OF THE ADJUSTABLE DAMPER

The gas-pressurized damper under investigation is a commercially available unit normally used on saloon car rallying or racing vehicles. The damper has 20 discrete

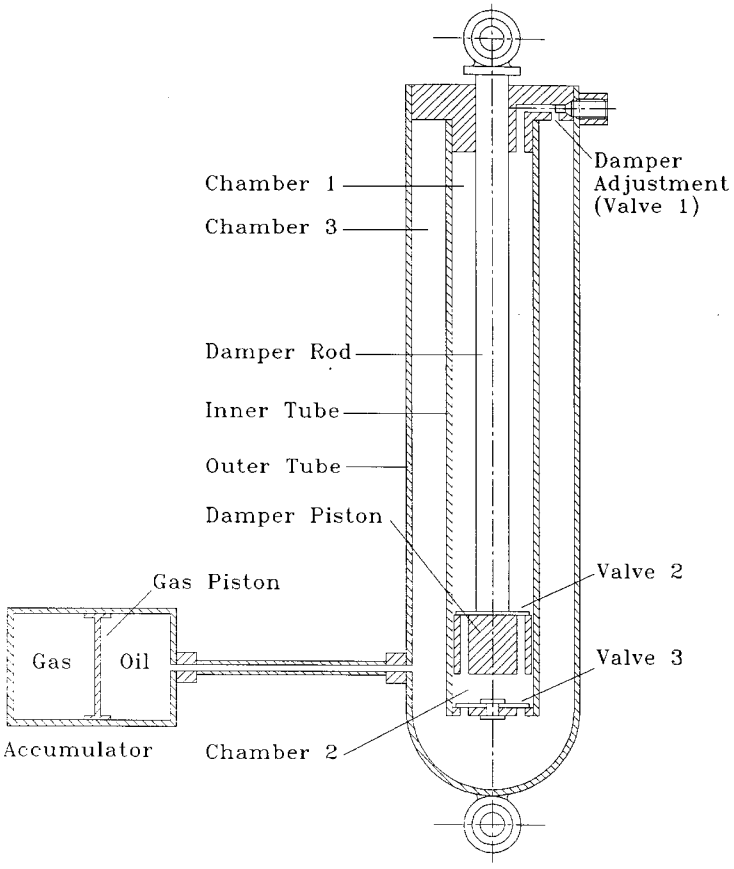

Fig. 1 Diagrammatic representation of the adjustable damper

settings that modify both the bump and rebound characteristics.

A sectioned diagram of the damper is shown in Fig. 1. The damper consists of two tubes, which are both filled with fluid and linked by three valves. The outer tube is connected by a flexible pipe to an accumulator (gas spring). The damper rod runs through a bearing and seal into the inner tube and is connected to the piston. The unit is attached to the vehicle suspension system by rose joints.

The characteristics of the damper are adjusted by means of valve 1, which has a detent giving it twenty settings. Adjusting the damper opens or closes a port, thus modifying the restriction to the flow through it. Closing the port causes the damping to increase in both bump and rebound. At any particular setting, the port area is fixed and does not vary with the pressure difference across it. Valve 1 controls the flow of fluid between chambers 1 and 3.

The flow through the piston is controlled by valve 2. Valve 2 allows flow in one direction only, from chamber 2 into chamber 1, and flow is prevented in the other direction. Thus, flow through this valve only occurs when the pressure in chamber 2 is greater than in chamber 1. The characteristics of this valve are complex because an attempt has been made, by the designer, to linearize the flow relationship. This has been achieved by allowing the flow area to change with the pressure difference across it.

The flow between chambers 3 and 2 is controlled by valve 3. This valve only allows flow from chamber 3 into 2, when the pressure in 3 is greater than in 2, and prevents any reverse flow. The flow area of this valve also varies with the pressure difference across it. The accumulator is connected, via a flexible pipe, to chamber 3 and acts to maintain a minimum damper pressure and as a reservoir for the fluid during operation.

The principle of operation of the damper will be considered by examining the two phases of operation: bump and rebound. During bump, the damper rod is moving into the unit. Flow through valve 3 is prevented because the pressure in chamber 2 is greater than in 3. Flow only occurs through valves 1 and 2. In rebound, the rod is being extracted from the damper. Flow occurs through valve 1 and 3 only, and there is no flow through valve 2.

The inner tube of this damper self-bleeds because the flow through valve 1 is always in the same direction, out of chamber 1, and the valving causes the damper to behave as a pump. Only in exceptional circumstances would the flow be reversed. Thus, any air or vapour that has collected at the top of the inner tube is flushed out during operation. The damping force is generated by the pressures in chambers 1 and 2 acting on the piston and any friction present in the bearings and seals. A full set of data for the adjustable damper under investigation are given in Table 1.

Table 1 Data for the adjustable damper

Damper parameter	Value
d_r	0.019 m
d_p	0.0285 m
d_g	0.04 m
l_1	0.133 m
l_2	0.133 m
l_g	0.05
ρ_0	770 kg m^2

3 THEORETICAL DAMPER MODEL

In this section a mathematical model of the adjustable damper is developed. The model proposed by Lang [**1**] is too complex for design or general simulation purposes but includes the compressibility of the fluid and cavitation (pressure falling to zero). While the model of reference [**6**] is much simpler, and also includes the fluid compressibility, it does not represent the design of commonly used dampers. The model developed in the present work uses a simplified version of the cavitation model given in reference [**1**], but deviates from references [**1**] and [**2**] in that it uses mass conservation to formulate the equations of motion. A suitable diagram for developing the mathematical model is shown in Fig. 2.

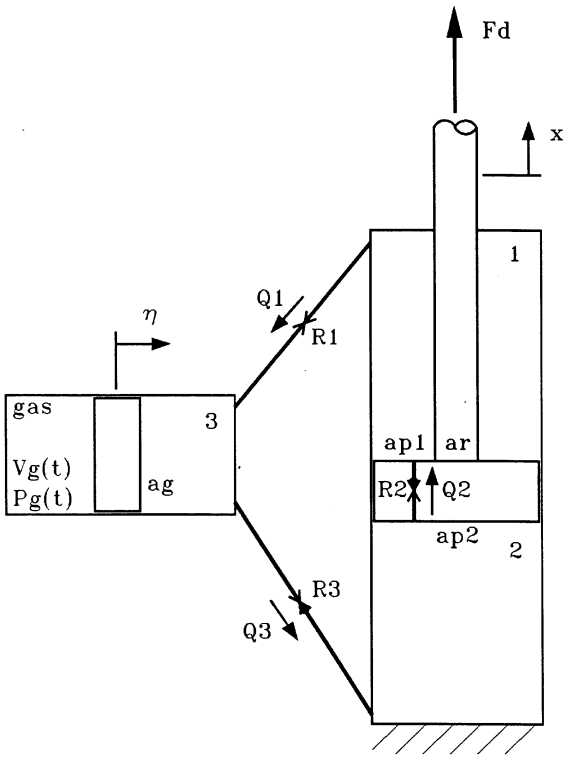

Fig. 2 Mathematical model of the adjustable gas-pressurized damper

The mathematical model of the damper is developed with the following assumptions:

1. The temperature is constant.
2. An effective bulk modulus is used to account for the compressibility of the oil and any trapped gas or vapour, and the expansion of the mechanical components in chambers 1 and 2 (Appendix 1).
3. The compressibility of the fluid in volume 3 is neglected because there is only a small change in pressure.
4. The vapour pressure of the oil is taken as $0\,\mathrm{N/m^2}$ and any vapour phase collapses immediately when the pressure is greater than this value [**1**].
5. Valves 2 and 3 are ideal one-way valves and the mass flowrate through them is proportional to the pressure difference across them.
6. The mass flowrate through valve 1 is proportional to the square root of the pressure difference across.
7. The mass of the gas piston is negligible and has no friction.
8. The gas in the accumulator undergoes adiabatic compression and expansion.

3.1 Damper model without friction

Applying mass conservation to chamber 1 gives

$$m_1 = m_{10} - \int_0^t \dot{m}_{v1}\,\mathrm{d}t + \int_0^t \dot{m}_{v2}\,\mathrm{d}t \tag{1}$$

where m_1 and m_{10} are the current and initial mass in volume 1 respectively, and $\dot{m}_{v1}$ and $\dot{m}_{v2}$ are the mass flowrates through valves 1 and 2 respectively. Letting $\dot{m}_1$ be the total mass flowrate into chamber 1, this equation can be written as

$$m_1 = m_{10} + \int_0^t \dot{m}_1\,\mathrm{d}t \tag{2}$$

The capacity of chamber 1 is given by

$$V_1 = V_{10} - xa_{p1} \tag{3}$$

where V_1 and V_{10} are the current and initial volumes in chamber 1, x is the displacement of the damper piston with respect to the cylinder and a_{p1} is the effective area of the piston in chamber 1.

The density of the oil in chamber 1 is given by

$$\rho_1 = \frac{m_1}{V_1} \tag{4}$$

The linearized equation of state for a liquid [**7**] is given by

$$\rho = \rho_0\left[1 + \left(\frac{\partial\rho}{\partial P}\right)_T (P - P_0) + \left(\frac{\partial\rho}{\partial T}\right)_P (T - T_0)\right] \tag{5}$$

where ρ and ρ_0 are the current and initial densities, P and P_0 are the current and initial pressures and T and T_0 are the current and initial temperatures.

The isothermal bulk modulus and expansion coefficients for the fluid are defined respectively by

$$K_B = \rho_0\left(\frac{\partial P}{\partial\rho}\right)_T = -V_0\left(\frac{\partial P}{\partial V}\right)_T$$

and

$$\alpha = -\frac{1}{\rho_0}\left(\frac{\partial\rho}{\partial T}\right)_P = \frac{1}{V_0}\left(\frac{\partial V}{\partial T}\right)_P \tag{6}$$

The effective bulk modulus for the system K_e [**7**], which includes the effect of the fluid, trapped gas and expansion of the mechanical components, will be used for the damper (Appendix 1). For constant temperature, ignoring the effect of thermal expansion, the pressure in chamber 1 is given by

$$P_1 = K_e\left(\frac{\rho_1}{\rho_0} - 1\right) + P_0 \tag{7}$$

where P_1 is the current pressure in chamber 1.

Applying mass conservation to volume 2 gives

$$m_2 = m_{20} - \int_0^t \dot{m}_{v2}\,\mathrm{d}t + \int_0^t \dot{m}_{v3}\,\mathrm{d}t \tag{8}$$

where m_2 and m_{20} are the current and initial mass in chamber 2 respectively, and $\dot{m}_{v3}$ is the mass flowrate through valve 3. Letting $\dot{m}_2$ be the total mass flowrate into chamber 2, this equation can be written as

$$m_2 = m_{20} + \int_0^t \dot{m}_2\,\mathrm{d}t \tag{9}$$

The capacity of volume 2 is given by

$$V_2 = V_{20} + xa_{p2} \tag{10}$$

where V_2, V_{20} and a_{p2} are the current and initial volume and the piston area in chamber 2.

The density of the fluid in chamber 2 is given by

$$\rho_2 = \frac{m_2}{V_2} \tag{11}$$

The pressure of the fluid in chamber 2 is given by

$$P_2 = K_e\left(\frac{\rho_2}{\rho_0} - 1\right) + P_0 \tag{12}$$

where P_2 is the current pressure in chamber 2.

With no density change, the volume of fluid in chamber 3, V_3, is given by

$$V_3 = \frac{m_3}{\rho_0} \tag{13}$$

and the mass of fluid in chamber 3 by

$$m_3 = m_{30} + \int_0^t \dot{m}_{v1}\,\mathrm{d}t - \int_0^t \dot{m}_{v3}\,\mathrm{d}t \tag{14}$$

where m_3 and m_{30} are the current and initial masses in chamber 3 respectively. This equation can be written as

$$m_3 = m_{30} + \int_0^t \dot{m}_3 \, \mathrm{d}t \tag{15}$$

where $\dot{m}_3$ is the total mass flowrate into chamber 3.

The motion of the gas piston, η, is given by

$$\eta = \frac{V_3 - V_{30}}{a_g} = \frac{\int_0^t \dot{m}_3 \, \mathrm{d}t}{a_g \rho_0} \tag{16}$$

where V_{30} is the initial volume of chamber 3 and a_g is the effective gas piston area.

The gas pressure and hence the fluid pressure in chamber 3 is given by

$$P_3 = P_g = P_0 \left(\frac{V_{g0}}{V_{g0} + m_3/\rho_0} \right)^{\gamma} \tag{17}$$

where P_g is the current gas pressure, V_{g0} is the initial gas volume and γ is the adiabatic index.

The mass flowrates through the three valves are given by

$$\dot{m}_{v1} = \frac{\sqrt{P_1 - P_3}}{R_{m1}}$$

$$\dot{m}_{v2} = \begin{cases} \dfrac{P_2 - P_1}{R_{m2}}, & P_2 > P_1 \\ 0, & P_2 \leqslant P_1 \end{cases}$$

$$\dot{m}_{v3} = \begin{cases} \dfrac{P_3 - P_2}{R_{m3}}, & P_3 > P_2 \\ 0, & P_3 \leqslant P_2 \end{cases} \tag{18}$$

where R_{m1}, R_{m2} and R_{m3} are the mass flow coefficients for the valves.

The damper force, f_d, without friction is given by

$$f_d = P_1 a_{p1} - P_2 a_{p2} \tag{19}$$

3.2 Friction model

The friction model used in this study is taken from reference [**8**]. This friction model simulates both the kinetic (Coulomb) and static (stiction) friction characteristics. In this investigation the static friction has been set to zero.

3.3 Damper model with friction

Incorporating the frictional characteristics into the damper model results in the following equation:

$$f_d = P_1 a_{p1} - P_2 a_{p2} + f_f \tag{20}$$

where f_f is the friction force. A block diagram of the damper model with friction is shown in Fig. 3. The data used in the next section for the damper model are given in Table 1.

4 SIMULATED RESPONSE OF THE DAMPER MODEL

To investigate the performance of the theoretical damper model that has been developed, the parameters identified for setting number 10 (Section 6) will be used as a baseline for the purpose of comparison. This section

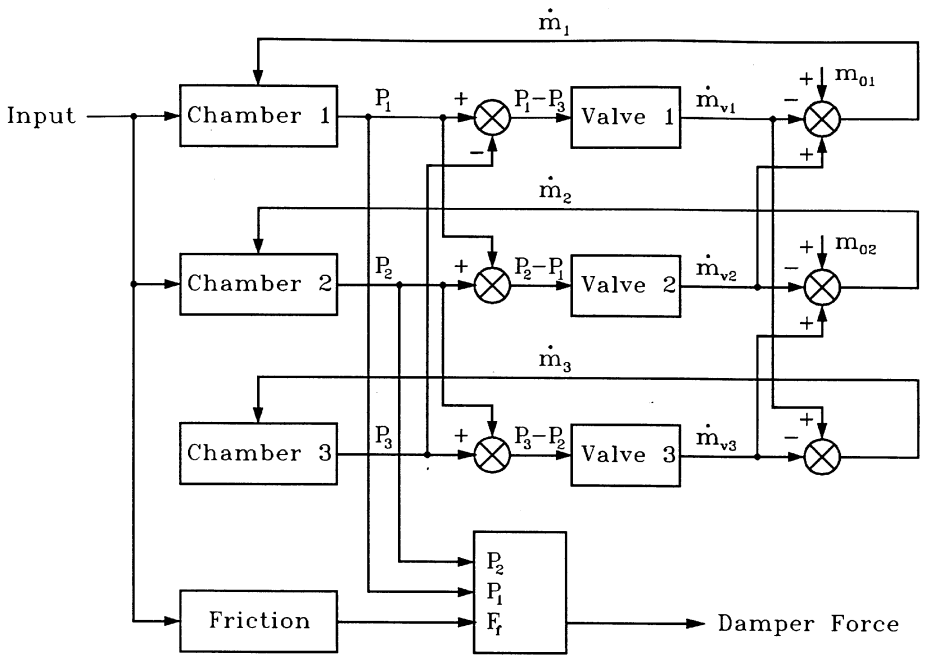

Fig. 3 Block diagram of the damper model

is broken down into three subsections, considering the effect of variations in the three valve coefficients, effective bulk modulus and kinetic friction.

4.1 Effect of variation in the valve coefficients

The effect of varying the coefficients for the three valves is examined in this section. A simplified model of the adjustable damper is referred to when discussing the responses; this model is given in Appendix 2.

4.1.1 Variation in valve 1 coefficient

The effect of varying the mass flow coefficient for valve 1, R_{m1}, by ± 20 per cent is shown in Fig. 4. The central region of the curve has not been affected by the variations in the valve coefficient considered.

Reducing the coefficient has caused a lowering of the force being developed in both bump and rebound. The effect is greater in rebound than in bump. The compressibility of the fluid is less evident because the amount of hysteresis in the curve has been reduced [3].

Increasing the coefficient has resulted in an increase in the damper force in both bump and rebound. Again, the effect is more evident in rebound. There is also an increase in the hysteresis, indicating that the compressibility of the fluid is playing a larger part at the high pressure.

The simple model of this damper, given in Appendix 2, predicts a proportional increase in both the bump and

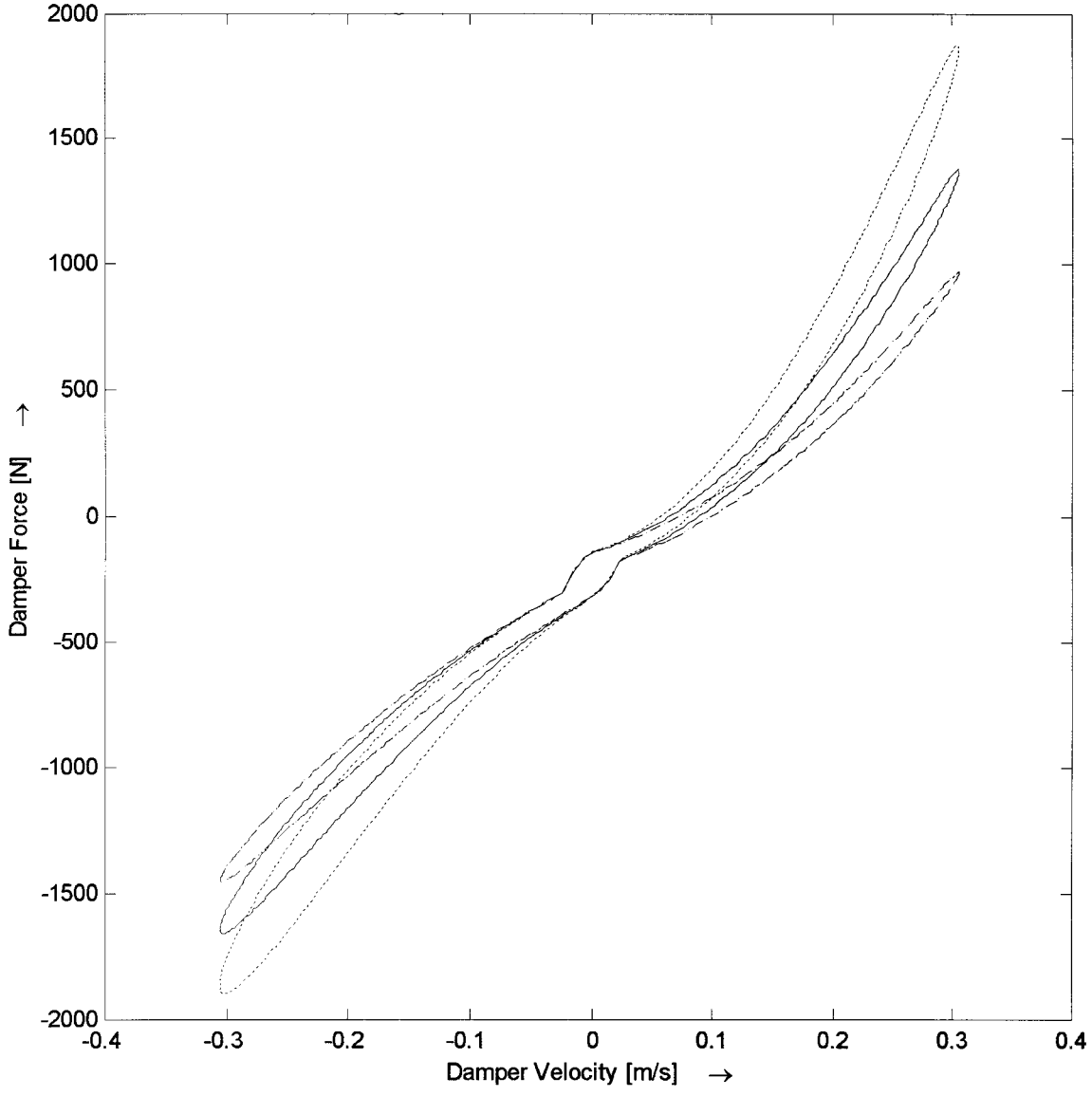

Fig. 4 Plot of the theoretical damper force against velocity for variations in R_{m1} for setting 10, R_{m1}^{s10}: —R_{m1}^{s10}; ———— $0.8 \times R_{m1}^{s10}$; $\cdots 1.2 \times R_{m1}^{s10}$

rebound force with valve coefficient. It also indicates that the rebound will be affected more than the bump because $a_{p1} > a_r$ for this damper (Table 1).

4.1.2 *Variation in valve 2 coefficient*

The effect of varying the mass flow coefficient for valve 2, R_{m1}, by ± 20 per cent is shown in Fig. 5. For the variations considered there has been no visible effect on the central region or rebound characteristic. This is expected from the simple model of Appendix 2.

Increasing the valve coefficient has caused the damper to generate higher forces in bump only. The hysteresis has also become larger, caused by the higher pressure within the fluid. Reducing the coefficient results in a lower damper force and hysteresis.

4.1.3 *Variation in valve 3 coefficient*

The effect of changing the mass flow coefficient for valve 3, R_{m3}, by ± 50 per cent is shown in Fig. 6. There is no visible effect on the central region or bump characteristics caused by these variations. The only effect is on the rebound. Reducing the coefficient causes a reduction in the force developed by the damper in rebound.

Increasing the coefficient has caused a dramatic change in the rebound characteristic. The effect of this change is worth investigating further. Examining the pressure in chamber 2 (Fig. 7) shows that it goes to zero during part of the rebound stroke. This is caused by the flow through valve 3 being insufficient to keep chamber 2 filled with fluid during this part of the stroke. Thus, the model is predicting that cavitation will occur in chamber

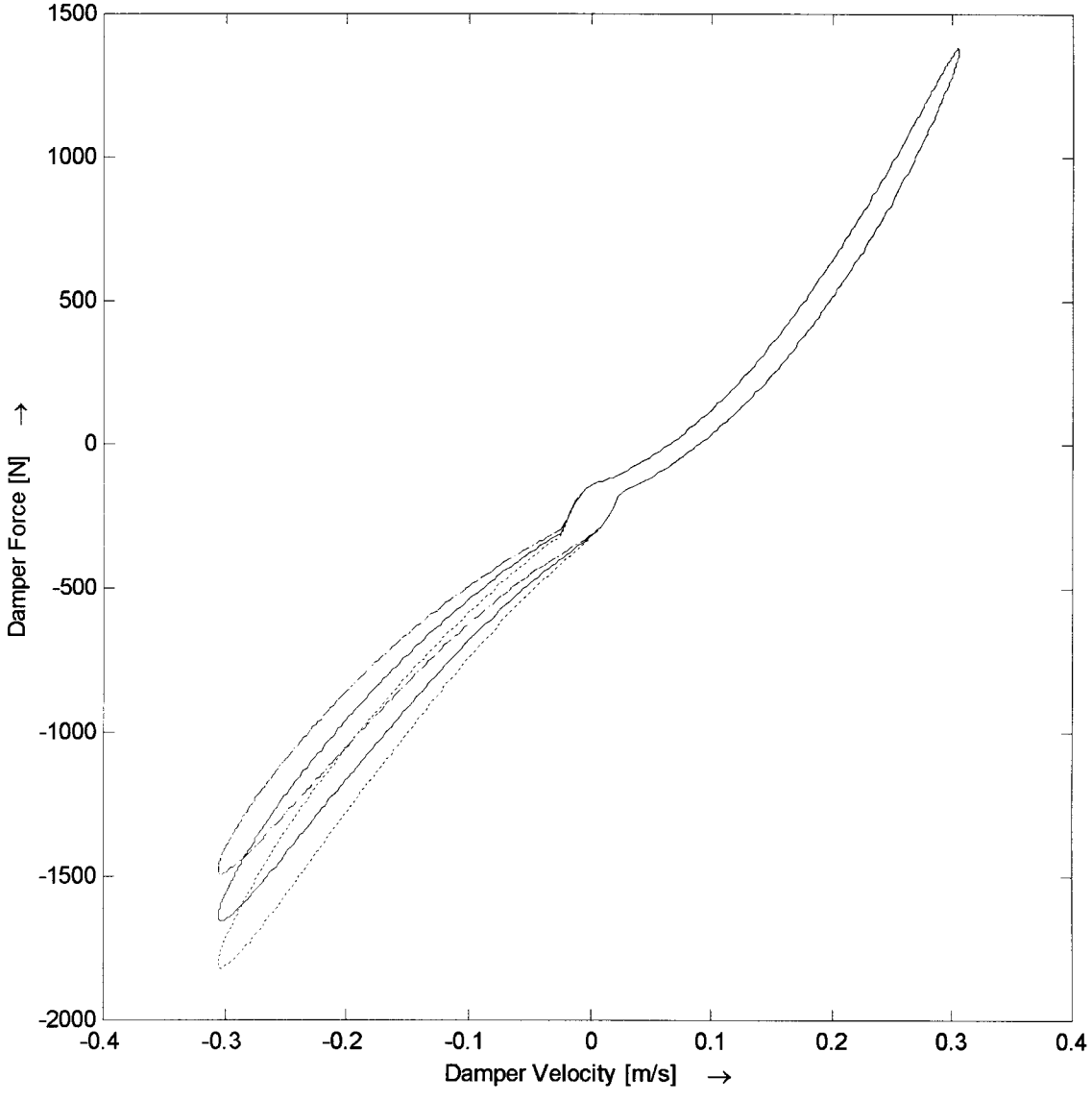

Fig. 5 Plot of the theoretical damper force against velocity for variations in R_{m2} for setting 10, R_{m2}^{s10}: —R_{m2}^{s10}; ———— $0.8 \times R_{m2}^{s10}$; $\cdots$ $1.2 \times R_{m2}^{s10}$

2. In normal operation this effect would cause problems for the operation of the damper.

The model given in Appendix 2 does not capture the cavitation phenomena without modification, though it does indicate that only rebound should be affected.

4.2 Effect of variation in the effective bulk modulus

The result of increasing the effective bulk modulus by 100 per cent and reducing it by 80 per cent is shown in Fig. 8. Increasing the value has had very little effect on the curve and the hysteresis has been slightly reduced, while reducing its value has had a significant effect. The hysteresis in the curve has increased by a factor of about 4.

4.3 Effect of variation in the kinetic (Coulomb) friction

In Fig. 9, the effect on the central region for three values of kinetic friction is shown. These values are 0, 50 (setting 10) and 100 N. These changes have altered primarily the central region and caused the offset between the bump and rebound characteristics to vary.

Without any kinetic friction there is a relatively smooth transition between the bump and rebound characteristics. Increasing the kinetic friction causes a

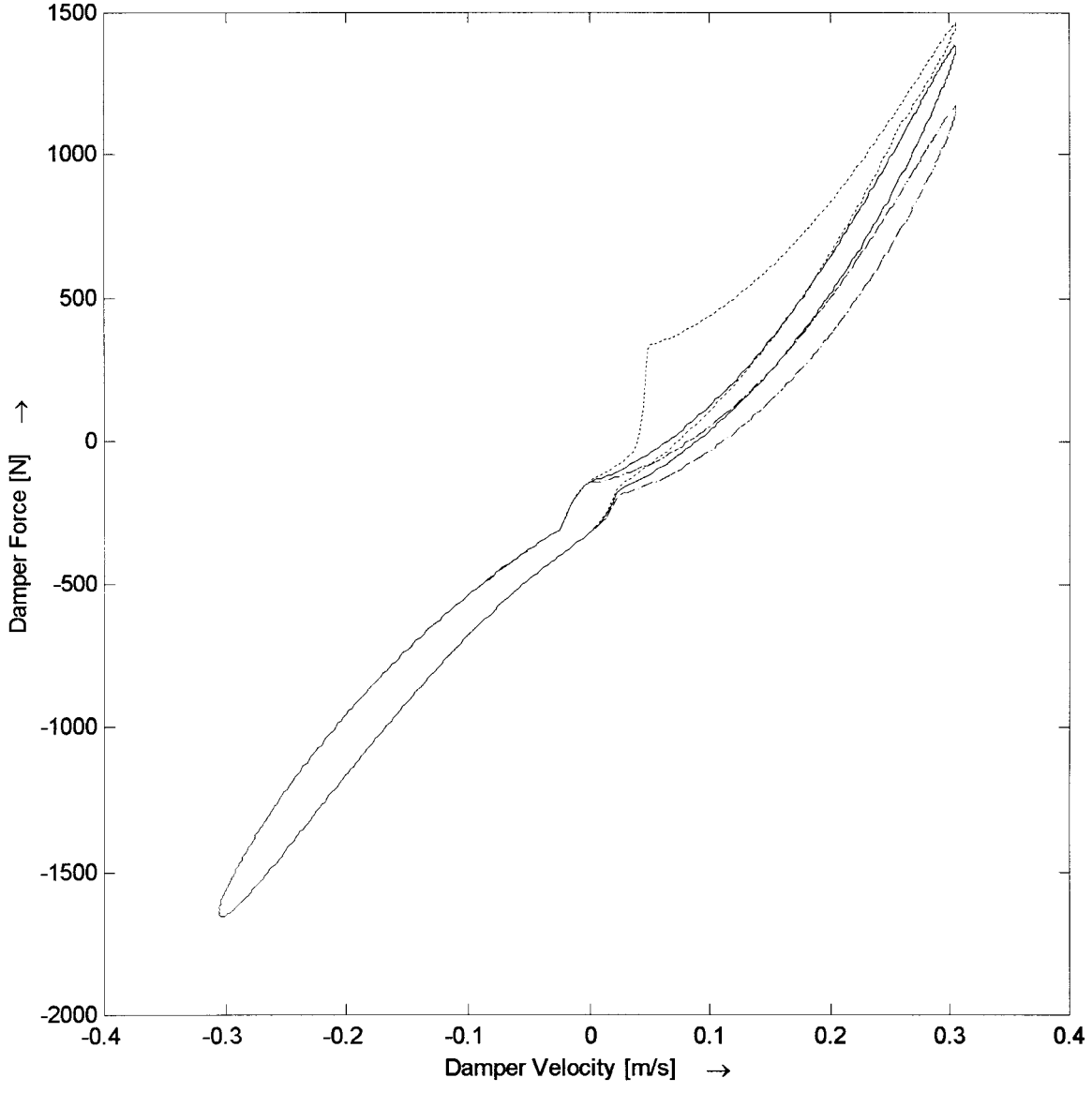

Fig. 6 Plot of the theoretical damper force against velocity for variations in R_{m3} for setting 10, R_{m3}^{s10}: —R_{m3}^{s10}; ———— $0.5 \times R_{m3}^{s10}$; $\cdots$ $1.5 \times R_{m3}^{s10}$

proportional increase in the offset between these two regions.

5 EXPERIMENTAL DAMPER RESPONSES

This section describes the experimental method used to test the damper. The best method for testing a damper would be to replicate the kinematics of the suspension system in which it is to be used. The experimental complexity involved with this is far too difficult for routine testing. The most common method employed in the literature [**4**, **5**, **9**, **10**] is to 'ground' one side of the damper, thereby neglecting some of the dynamics of the damper under test.

In the experimental work undertaken for this research, the lower end of the damper was 'grounded' to the frame of the test facility, the upper end being attached to a hydraulic actuator, as shown in Fig. 10. A force transducer between the lower end of the damper and frame was used to measure the force generated by the damper. The displacement transducer, within the actuator, was used to measure the motion of the damper. The velocity across the damper was derived from this displacement signal. The temperature of the outer damper tube was monitored during the testing. No pressure measurements from inside the unit were

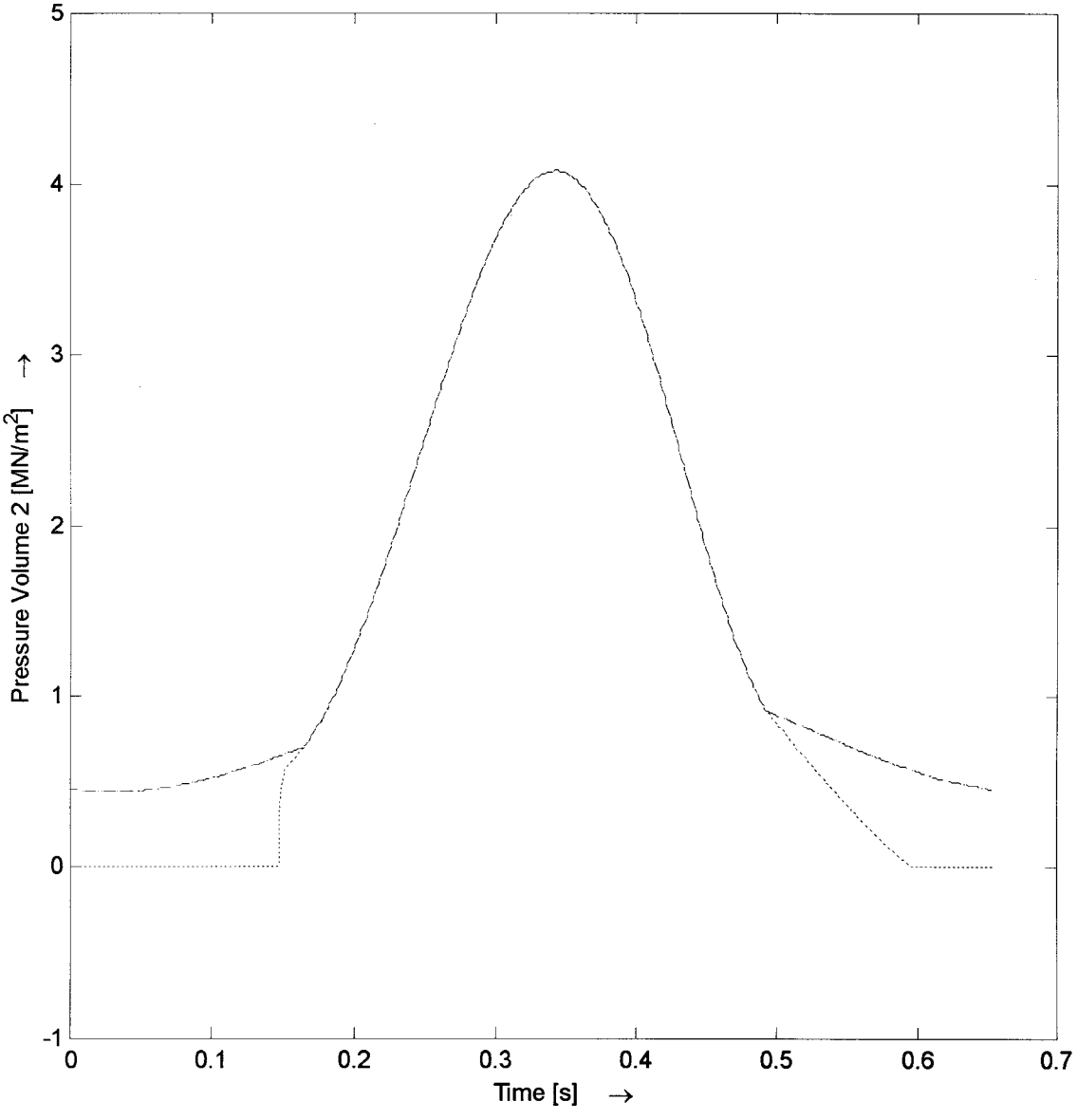

Fig. 7 Plot of the theoretical pressure in chamber 2 against time for variations in R_{m3} for setting 10, R_{m3}^{s10}: ——— $0.5 \times R_{m3}^{s10}$; $\cdots$ $1.5 \times R_{m3}^{s10}$

possible. This was because the damper was a commercially available unit and it was too difficult to get pressure sensors inside it. Both the force and displacement signals were low-pass filtered at 30 Hz with a fourth-order Butterworth filter to prevent aliasing.

Under continuous operation, the effects of temperature can cause the characteristics of the damper to vary dramatically [**11**]. To prevent this having too large an effect, sinusoidal rather than random testing was performed. The tests were conducted at 1.5 Hz with an amplitude of 0.032 m. During the testing, the outer tube temperature of the damper was held at $26 \pm 1\,^{\circ}\mathrm{C}$ by forced air cooling. To further minimize temperature effects, only 15 cycles were captured at each setting. Plots of the results from the testing at settings 5 and 10 are shown in Figs 11 and 12.

6 PARAMETER IDENTIFICATION FOR THE MODEL

In this section the method used to estimate the parameters for the adjustable damper and the results obtained are discussed.

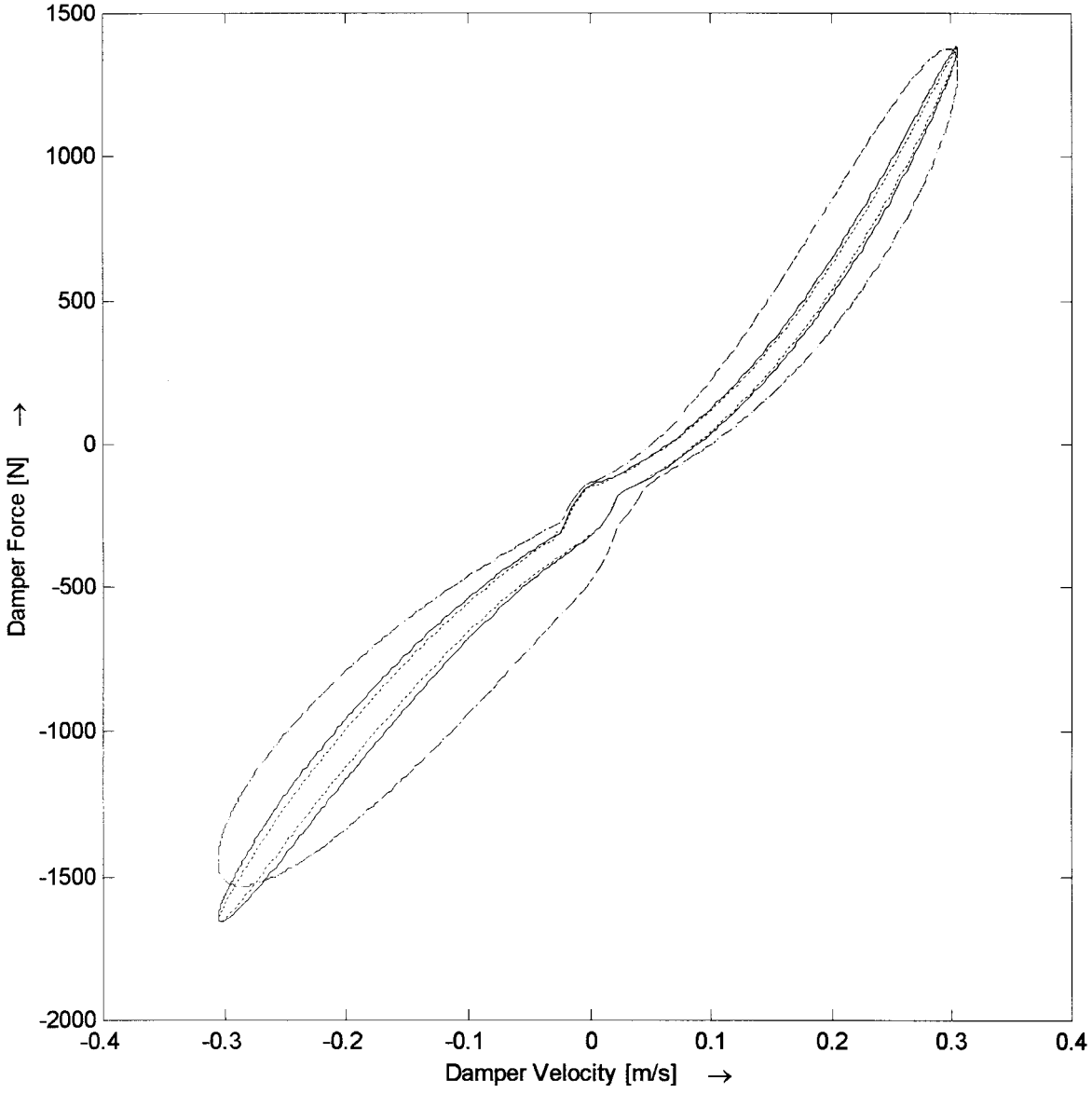

Fig. 8 Plot of the theoretical damper force against velocity for variations in K_e for setting 10, K_e^{s10}: — K_e^{s10}; ——— $0.2 \times K_e^{s10}$; $\cdots 2 \times K_e^{s10}$

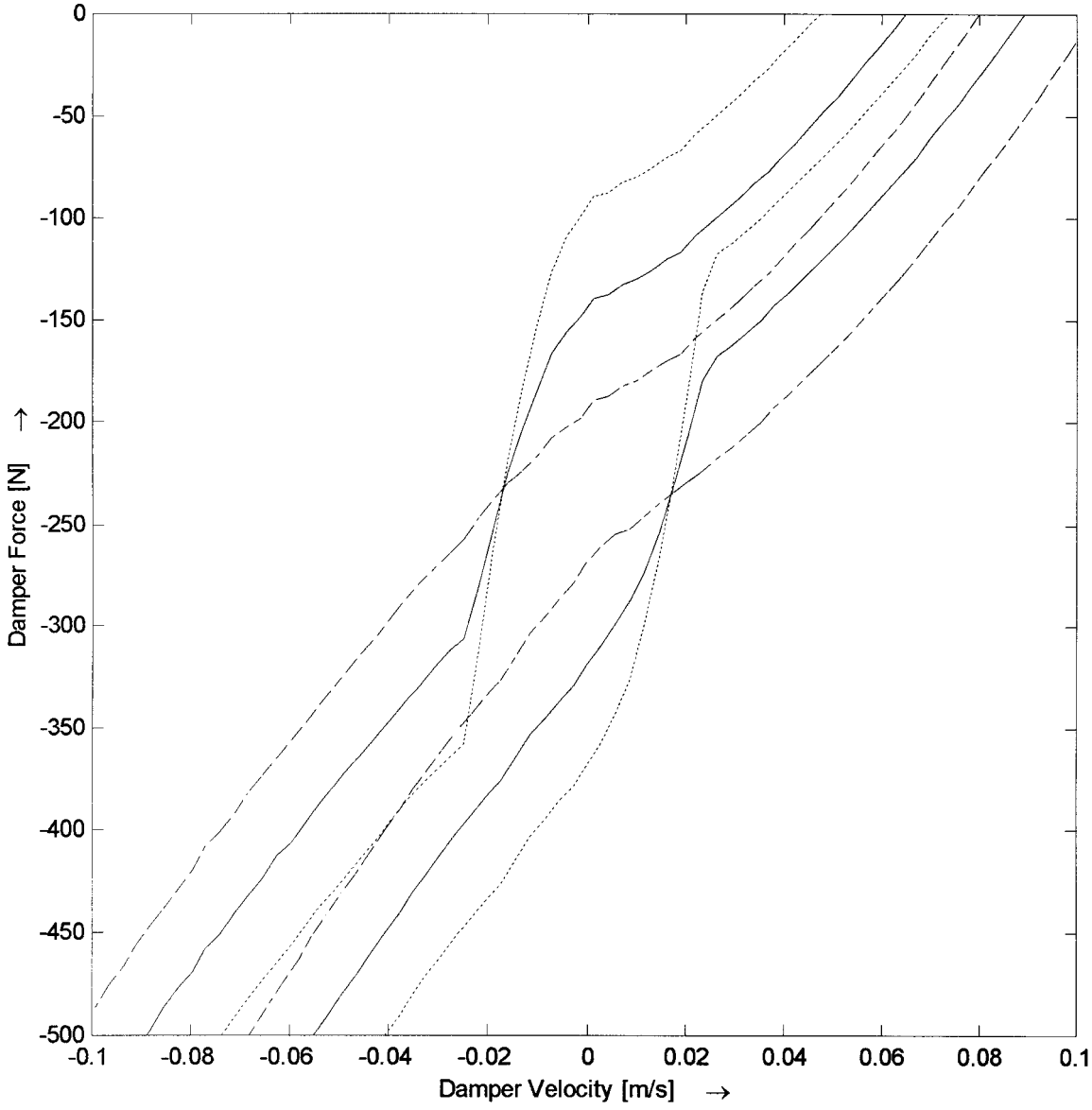

Fig. 9 Plot of the theoretical damper force against velocity for variations in f_f for setting 10 (50 N): — $f_f = 50$ N; ——— $f_f = 0$ N; $\cdots$ $f_f = 100$ N

6.1 Identification method

The method selected to fit the simulated model data to those obtained from the experiment was a least squares multiobjective technique, which minimized the following relationship:

$$\tfrac{1}{2}\|\hat{f}_d(y) - f_d\|_2^2 \tag{21}$$

where $y = [R_{m1}, R_{m2}, R_{m3}, K_e, f_f]^T$, and f_d and $\hat{f}_d$ are the measured and simulated damper forces as a function of time. The method employed to minimize equation (21) was that of Levenberg–Marquardt [**12**].

The quality of the model fit has been examined using the normalized mean square error (MSE). This technique has been used for assessing the quality of fit between damper models and experimental data in references [**13**] and [**14**]. The equation for the normalized MSE criterion is

$$\mathrm{MSE}(f_d) = \frac{100}{N\sigma_{f_d}^2}\sum_{i=1}^{N}(f_{di} - \hat{f}_{di})^2 \tag{22}$$

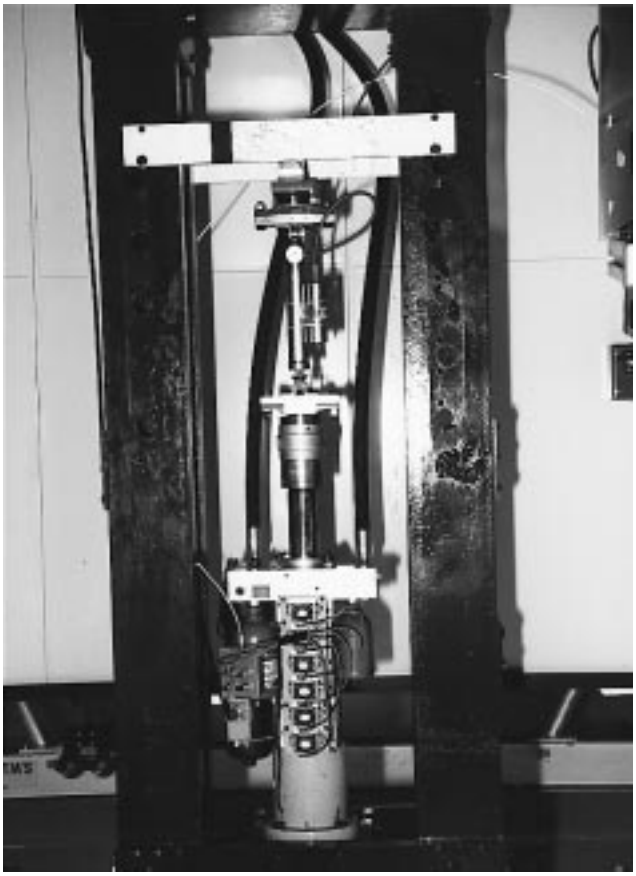

Fig. 10 Photograph of the experimental test facility

where N is the number of samples and σ_{f_d} is the standard deviation of the measured data. A guide to the quality of the model fit [**14**] can be summarized as follows:

1. A normalized MSE < 5 per cent indicates a good model fit.
2. A normalized MSE < 1 per cent indicates an excellent model fit.

6.2 Identification of the damper parameters

Using the experimental data for the damper, the mass flow coefficients for valves 1 and 2 and the effective bulk modulus have been estimated for each damper setting. During the initial investigation it was found that the value for the kinetic friction did not vary much with damper setting. Thus, it was decided to fix its value at 50 N, which was close to its mean value over the 20 settings. The mass flow coefficient for valve 3 was fixed at 2.597 MN s/m^2 kg because it was found that at the higher damper settings the minimization routine increased its value to a point where cavitation was occurring in chamber 2. The value chosen is the one identified for setting 1, which is about 15 per cent below the value at which cavitation occurs.

The normalized MSE for the model parameters identified against damper setting is shown in Fig. 13. From this plot it can be seen that it remains below 1 per cent for all the damper settings. Thus, from the criteria of Section 6.1, this indicates an excellent model fit. Plots of the parameters identified for the damper against setting are shown in Figs 14 to 16.

The plots of valve coefficients (Figs 14 and 15) show a smooth accelerating increase with setting. The plot for valve 2 (Fig. 15) shows a much more rapid increase at the higher settings. Both plots show a sudden change for setting 20. The cause of the change is unknown at present but is thought to be caused by the method of adjusting the port size in valve 1.

The plot of effective bulk modulus (Fig. 16) is fairly erratic. This may be due to the model not fully capturing the dynamics of the damper and the effective bulk modulus being used as a tuning parameter. Fitting a quadratic, by least squares, to the plot (Fig. 16) shows a possible increase in modulus with setting and hence pressure. This type of relationship would be expected if the fluid contained trapped air or vapour (Appendix 1).

Two of the results, settings 5 and 10, for the simulated and measured damper force against velocity are shown in Figs 11 and 12. These two plots show the closeness of the model fit to the experimental data.

7 CONCLUSION

A model of an adjustable damper has been presented. The model has been formulated with tuneable parameters relating to the valves, effective bulk modulus and friction. Only the parameters for valves 1 and 2 and the effective bulk modulus have been used for tuning the model because of cavitation problems caused by large values for the coefficient for valve 3 and only small variations in the level of kinetic friction occurring between settings.

The model proposed has been shown to capture the dominant dynamic behaviour of the damper at each setting, with the parameters selected. The parameters for the model have been selected using a multiobjective minimization problem, which has resulted in an excellent model fit to the experimental data.

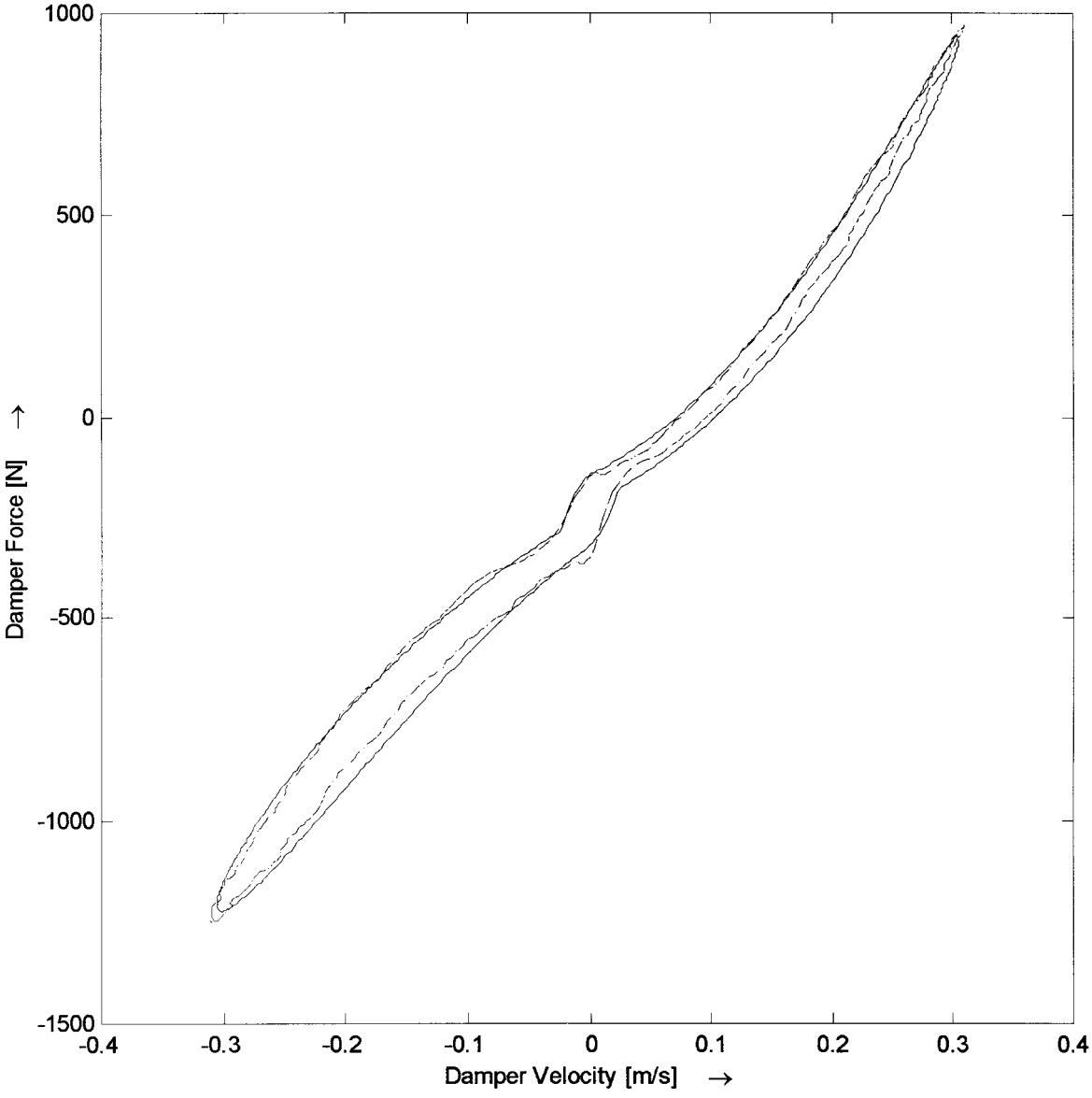

Fig. 11 Plot of the damper force against velocity for setting 5: — theoretical; – – – experimental

REFERENCES

1 **Lang, H. H.** A study of the characteristics of automotive dampers at high stroking frequencies. PhD thesis, Department of Mechanical Engineering, University of Michigan, 1977.

2 **Hall, B. B.** and **Gill, K. F.** Performance of a telescopic dual-tube automotive damper and the implications for vehicle ride prediction. *Proc. Instn Mech. Engrs, Part D, Journal of Automobile Engineering*, **200**(D2), 1986.

3 **Karadayi, R.** and **Masada, G. Y.** A nonlinear shock absorber model. In Proceedings of ASMS Symposium on *Simulation and Control of Ground Vehicles and Transportation Systems*, 1986, AMD-Vol. 80, DSC-Vol. 2.

4 **Hagedorn, P.** and **Wallaschek, J.** On equivalent harmonic and stochastic linearization for nonlinear shock-absorbers. In Proceedings of Nonlinear Stochastic Dynamic Engineering Systems IUTAM Symposium, Innsbruk/Igls, Austria, 21–26 June 1987.

5 **Wallaschek, J.** Dynamics of non-linear automobile shock-absorbers. *Int. J. Non-Linear Mech.*, 1990, **25**(2/3), 299–308.

6 **Surace, C., Worden, K.** and **Tomlinson, G. R.** An improved nonlinear model for an automotive shock absorber. *Nonlinear Dynamics*, 1992, **3**, 413–429.

7 **Merrit, H. E.** *Hydraulic Control Systems*, 1967 (John Wiley).

8 **Haessig, D. A.** and **Friedland, B.** On the modeling and simulation of friction. *Trans. ASME, J. Dynamic Syst.*,

Measmt and Control, 1991, **113**, 354–362.

9 **Belingardi, G.** and **Campanile, P.** Improvement of the shock absorber dynamic simulation by the restoring force mapping method. In Proceedings of 15th International Seminar on *Modal Analysis and Structural Dynamics*, Leuven, Belgium, 1990.

10 **Cafferty, S.** and **Tomlinson, G. R.** Characterization of automotive dampers using higher order frequency response functions. *Proc. Instn Mech. Engrs, Part D, Journal of Automobile Engineering*, 1997, **211**(D3), 181–203.

11 **Surace, C., Storer, D.** and **Tomlinson, G. R.** Characterising an automotive shock absorber and the dependence on temperature. In Proceedings of the 10th International Conference on *Modal Analysis*, San Diego, California, 1992, pp. 1317–1326.

12 *Matlab, Simulink and Optimisation Toolbox* (The Mathworks, Inc., Natick, Massachusetts).

13 **Worden, K.** Data processing and experimental design for the restoring force surface method, Part I: integration and differentiation of the measured time data. *Mech. Syst. and Signal Processing*, 1990, **4**(4), 295–319.

14 **Cafferty, S.** Characterization of automotive shock absorbers using time and frequency domain techniques. PhD thesis, Department of Engineering, University of Manchester, 1996.

APPENDIX 1

Effective bulk modulus

The effective bulk modulus for the damper has been obtained as follows [7]. The effective bulk modulus for the system is given by

$$\frac{1}{K_e} = \frac{V_v}{V_t}\left(\frac{1}{K_g}\right) + \frac{V_f}{V_t}\left(\frac{1}{K_B}\right) + \frac{1}{K_c} \tag{23}$$

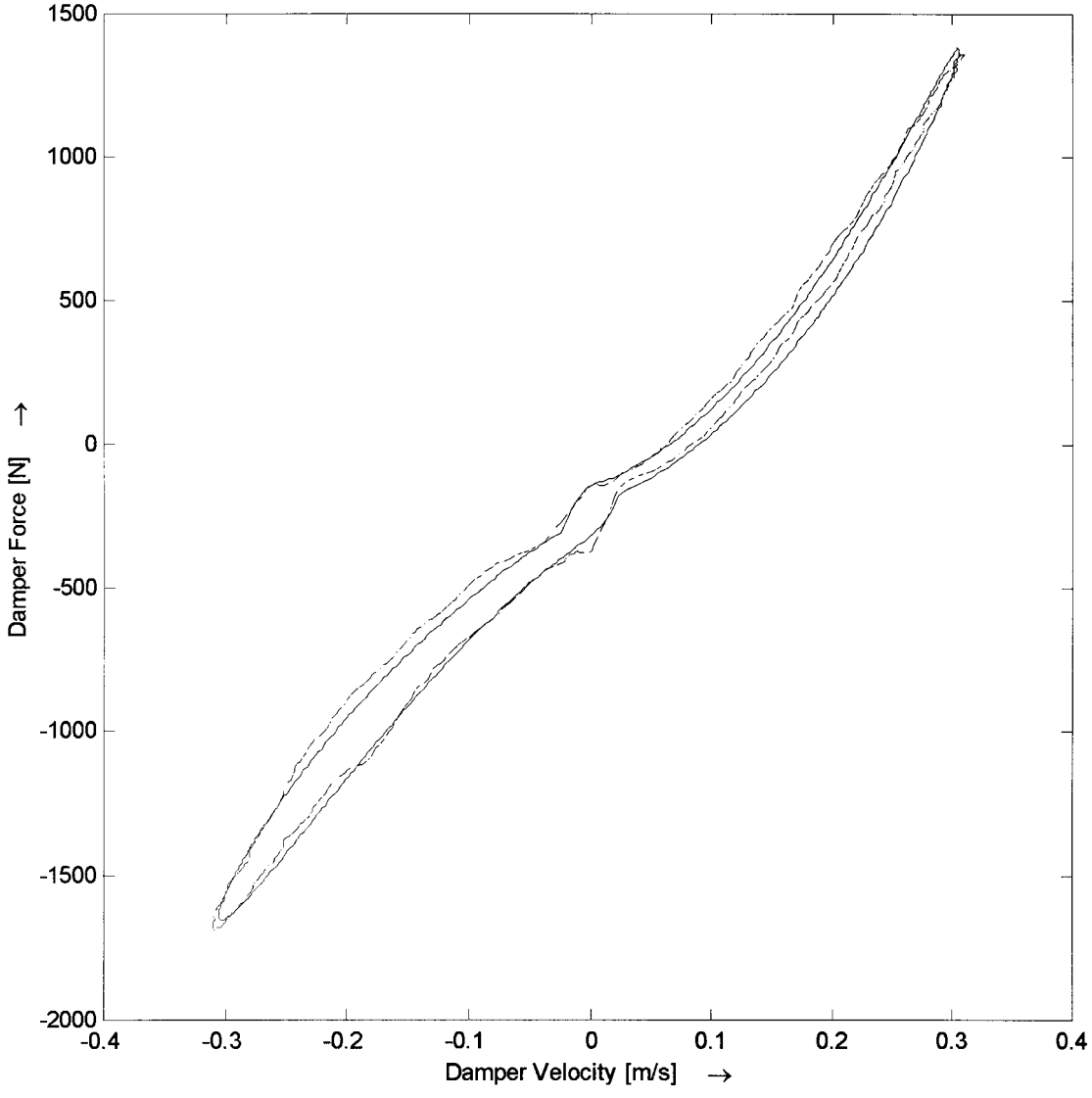

Fig. 12 Plot of the damper force against velocity for setting 10: — theoretical; – – – experimental

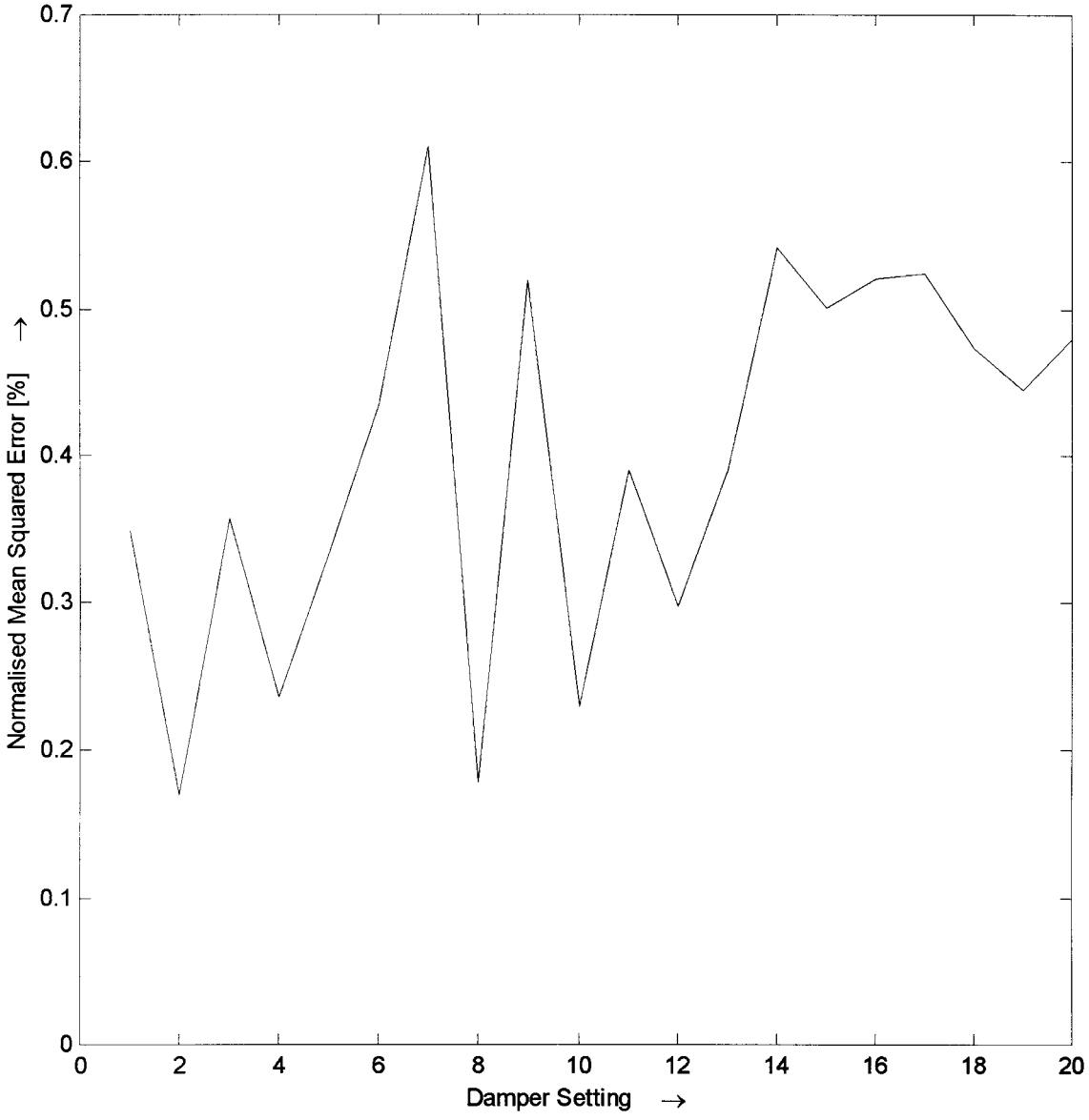

Fig. 13 Plot of the normalized MSE against the damper setting

where the total volume $V_t = V_f + V_v$, V_f and V_v are the volumes of the fluid and gas, and K_e, K_g, K_B and K_c are the bulk moduli for the system (effective), gas, fluid and cylinder.

Defining a volume ratio

$$V_r = \frac{V_v}{V_f} \tag{24}$$

results, after some algebraic manipulation, as

$$K_e = \frac{K_e K_B (1 + V_r)}{K_B V_r + K_g + K_g K_B (1 + V_r)/K_c} \tag{25}$$

or, assuming $V_r \ll 1$, gives

$$K_e = \frac{K_e K_B}{K_B V_r + K_g + K_g K_B / K_c} \tag{26}$$

From reference [7], the bulk moduli for the gas and cylinder are given by

$$K_g = \gamma P \qquad \text{and} \qquad K_c = \frac{t_c E}{D_i} \tag{27}$$

where t_c, E and D_i are the cylinder thickness, Young's modulus and inner diameter of the cylinder.

Equation (25) can be written as

$$K_e = \frac{K_B \gamma P}{K_B V_r + C\gamma P} \tag{28}$$

where

$$C = 1 + \frac{K_B D_i}{t_c E} \tag{29}$$

Consideration of equation (28) at low and high pressure gives

$$K_e|_{P\to 0} = 0 \qquad \text{and} \qquad K_e|_{P\to\infty} = \frac{K_B}{C} \tag{30}$$

Thus, the effective bulk modulus increases with pressure, which is caused by the effect of the gas or vapour.

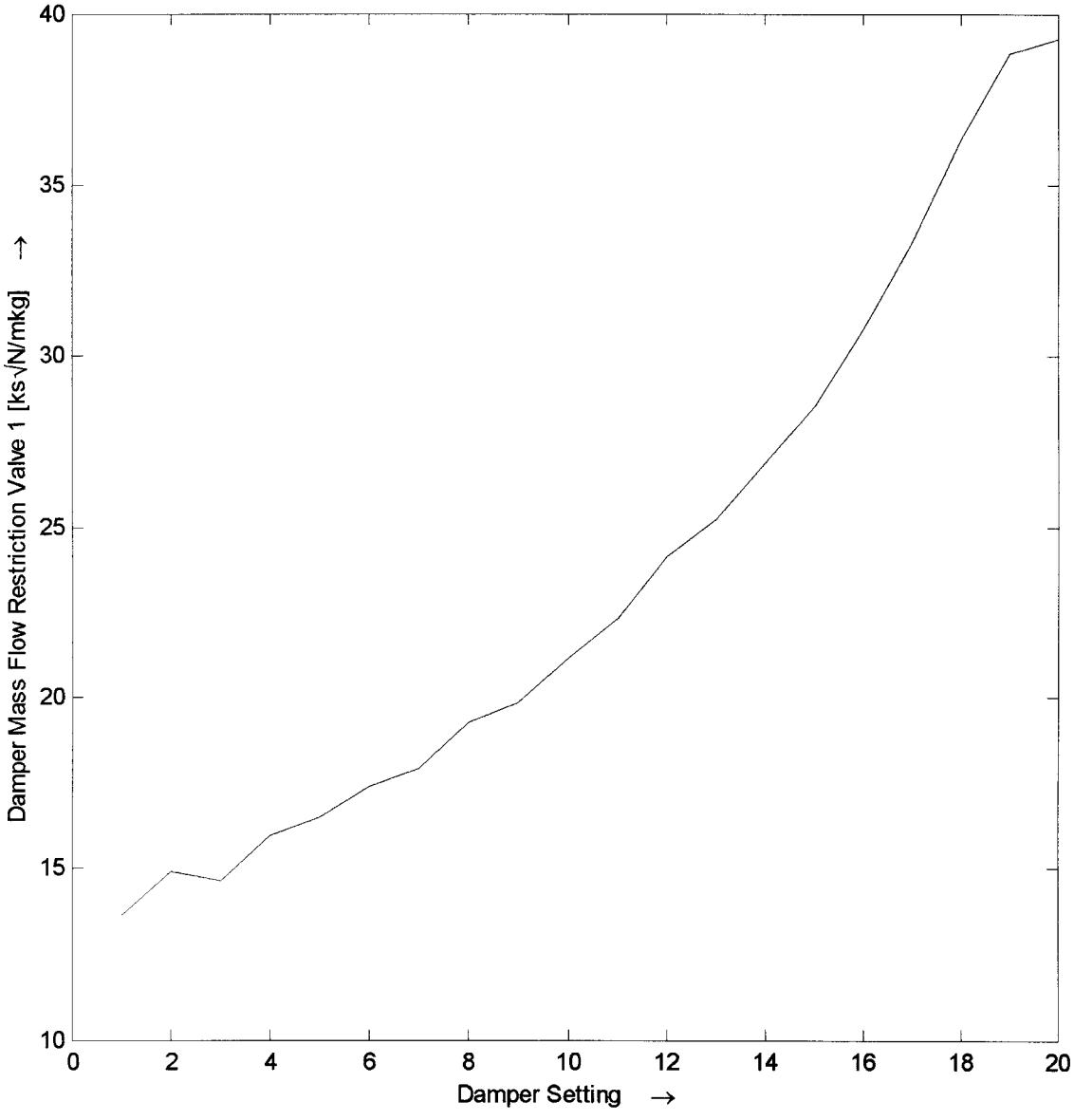

Fig. 14 Plot of the mass flow coefficient for valve 1, R_{m1}, against the damper setting

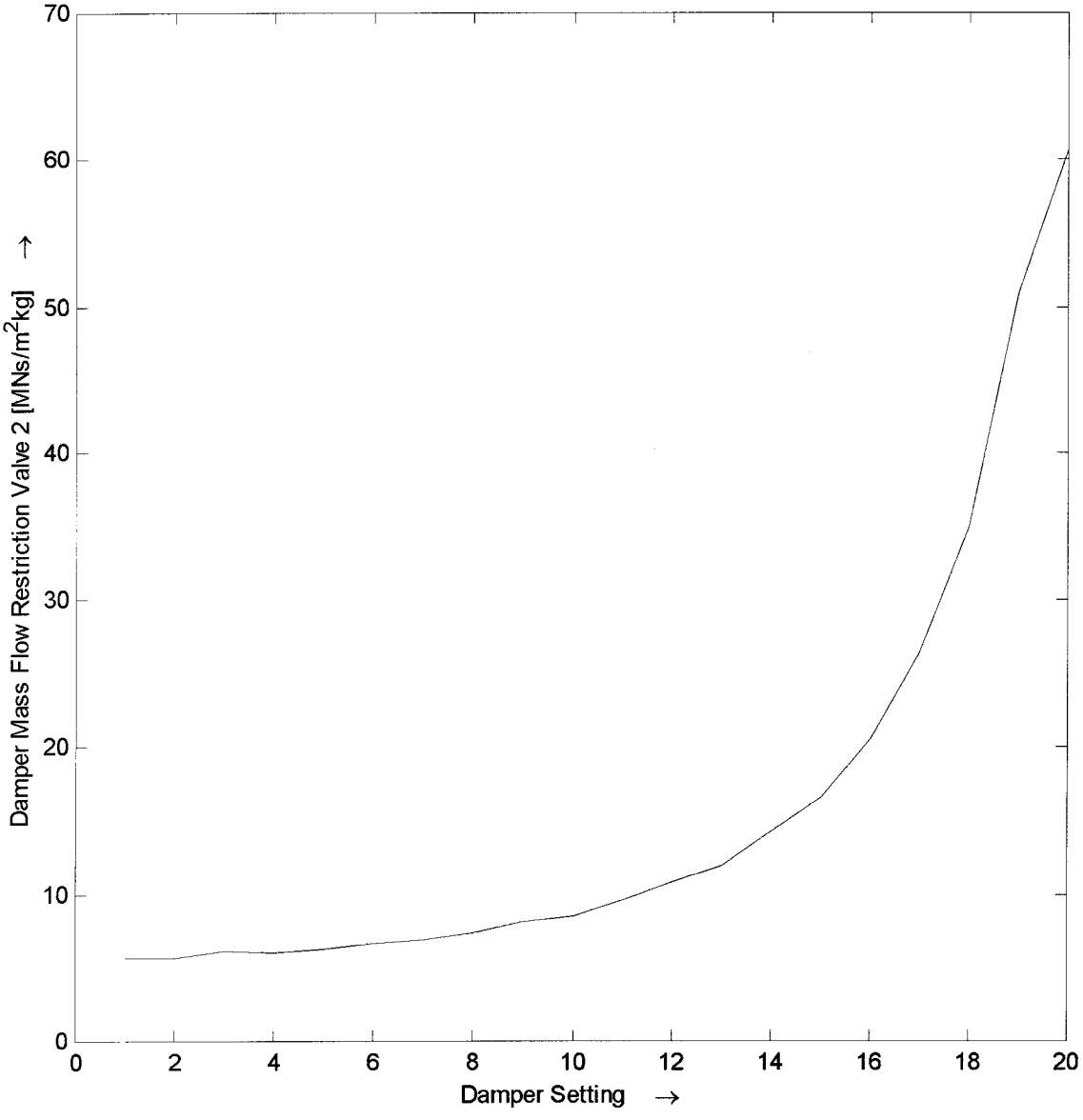

Fig. 15 Plot of the mass flow coefficient for valve 2, R_{m2}, against the damper setting

APPENDIX 2

Simple adjustable damper model

A simple mathematical model of the damper is developed with the following assumptions:

1. The oil is incompressible.
2. Valves 2 and 3 are perfect one-way valves.
3. The flow through the valves, when flow is possible, is proportional to the pressure difference across them.
4. The mass of the gas piston is negligible.
5. Friction is ignored.
6. The rod and cylinders are completely rigid.

With reference to Fig. 2, flow continuity in chamber 1 gives

$$q_1 = q_2 + \dot{x}a_{p1} \tag{31}$$

where q_1 and q_2 are the flows through valves 1 and 2 respectively.

Flow continuity in chamber 2 gives

$$q_3 = q_2 + \dot{x}a_{p2} \tag{32}$$

where q_3 is the flowrate through valve 3.

Flow continuity in chamber 3 gives

$$q_3 = q_1 + \dot{\eta}a_g \tag{33}$$

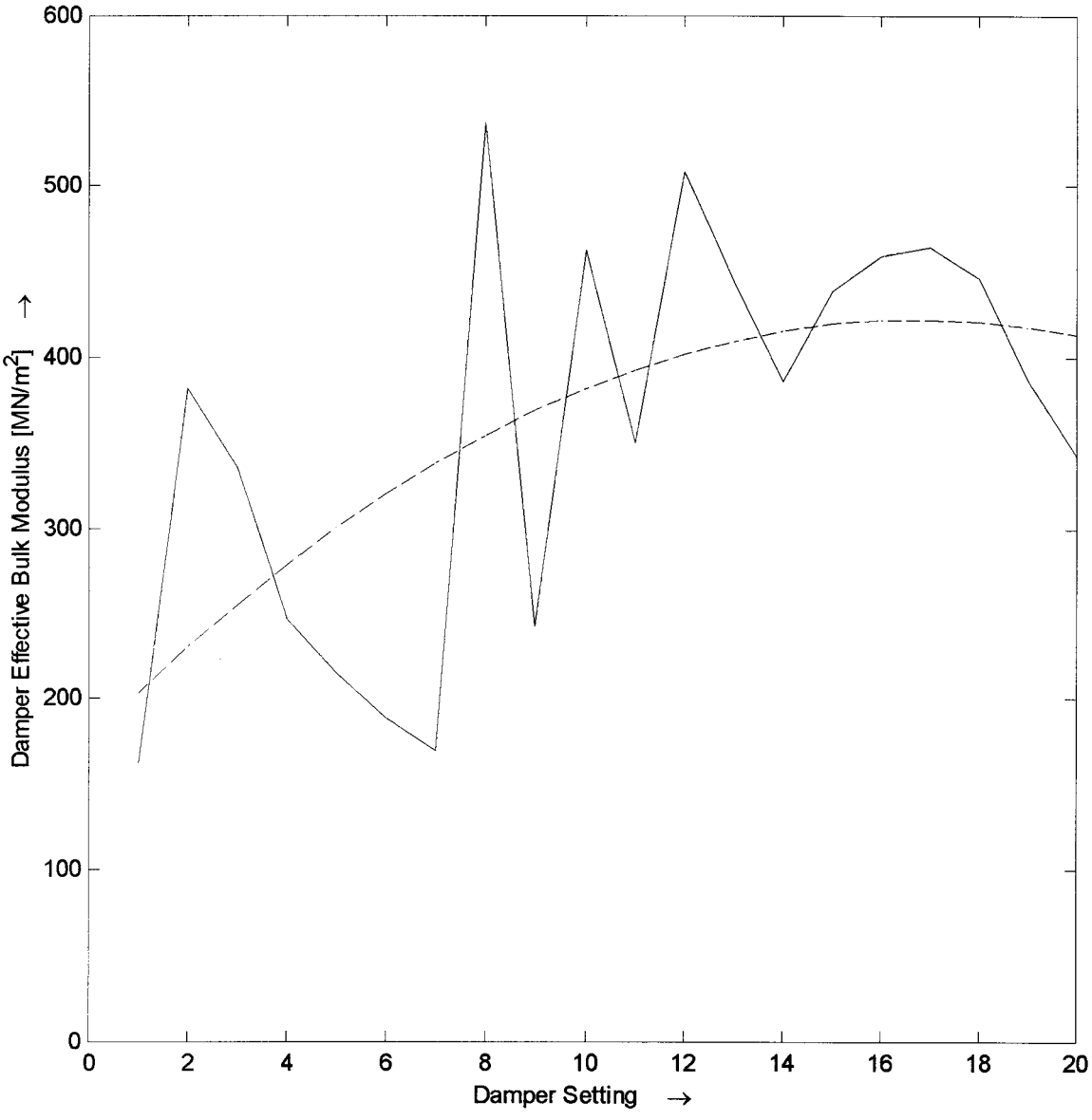

Fig. 16 Plot of the effective bulk modulus, K_e, against the damper setting: — estimated; – – – quadratic curve through estimated values

The flow relationships for valves 1, 2 and 3 are given by

$$q_1 = \frac{P_1 - P_3}{R_{v1}}$$

$$q_2 = \begin{cases} \dfrac{P_2 - P_1}{R_{v2}}, & P_2 > P_1 \\ 0, & P_2 \leqslant P_1 \end{cases}$$

$$q_3 = \begin{cases} \dfrac{P_3 - P_2}{R_{v3}}, & P_3 > P_2 \\ 0, & P_3 \leqslant P_2 \end{cases} \tag{34}$$

where R_{v1}, R_{v2} and R_{v3} are the flow restriction coefficients for valves 1, 2 and 3.

The relationship between the motion of the gas piston and the damper piston is given by

$$\eta = x\frac{a_r}{a_g} \tag{35}$$

where

$$a_r = a_{p2} - a_{p1} \tag{36}$$

The damper force is obtained from

$$f_d = P_1 a_{p1} - P_2 a_{p2} \tag{37}$$

The damper force is obtained from the above equations and is given by

$$f_{\mathrm{d}} = \begin{cases} \dot{x}(a_{\mathrm{p1}}^2 R_{\mathrm{v1}} + a_{\mathrm{p2}}^2 R_{\mathrm{v3}}) - P_3 a_{\mathrm{r}}, & \dot{x} > 0 \\ -a_{\mathrm{r}} P_3 & \dot{x} = 0 \\ \dot{x}(a_{\mathrm{p2}}^2 R_{\mathrm{v2}} + a_{\mathrm{r}}^2 R_{\mathrm{v1}}) - P_3 a_{\mathrm{r}}, & \dot{x} < 0 \end{cases} \tag{38}$$

For this model the damper force changes between positive and negative velocities. The slopes of the damper force with velocity are given by

$$c_{\dot{x}>0} = (a_{\mathrm{p1}}^2 R_{\mathrm{v1}} + a_{\mathrm{p2}}^2 R_{\mathrm{v3}})$$

$$c_{\dot{x}<0} = (a_{\mathrm{p2}}^2 R_{\mathrm{v2}} + a_{\mathrm{r}}^2 R_{\mathrm{v1}}) \tag{39}$$